Effect of torsional stiffness and inertia on the dynamics of low aspect ratio flapping wings

2014 Bioinspir. Biomim. 9 016008

(http://iopscience.iop.org/1748-3190/9/1/016008)

IOP Publishing Bioinspiration & Biomimetics
Bioinspir. Biomim. 9 (2014) 016008 (15pp) doi:10.1088/1748-3182/9/1/016008

Effect of torsional stiffness and inertia on the dynamics of low aspect ratio flapping wings

Qing Xiao[1], **Jianxin Hu**[1] **and Hao Liu**[2,3]

[1] Department of Naval Architecture and Marine Engineering, University of Strathclyde, 100 Montrose Street, Glasgow, G4 0LZ, UK
[2] Graduate School of Engineering, Chiba University, Chiba, 263-8522, Japan
[3] Shanghai-Jiao Tong University and Chiba University International Cooperative Research Centre (SJTU-CU ICRC), 800 Dongchuan Road, Minhang District, Shanghai, People's Republic of China

E-mail: qing.xiao@strath.ac.uk

Received 26 July 2013, revised 26 November 2013
Accepted for publication 6 December 2013
Published 16 January 2013

Abstract

Micro air vehicle-motivated aerodynamics in biological flight has been an important subject in the past decade. Inspired by the novel flapping wing mechanisms in insects, birds and bats, we have carried out a numerical study systematically investigating a three-dimensional flapping rigid wing with passively actuated lateral and rotational motion. Distinguishing it from the limited existing studies, this work performs a systematic examination on the effects of wing aspect ratio (AR = 1.0 to infinity), inertia (density ratio $\sigma = 4$–32), torsional stiffness (frequency ratio $F = 1.5$–10 and infinity) and pivot point (from chord-center to leading edge) on the dynamics response of a low AR rectangular wing under an initial zero speed flow field condition. The simulation results show that the symmetry breakdown of the flapping wing results in a forward/backward motion with a rotational pitching. When the wing reaches its stable periodic state, the induced pitching frequency is identical to its forced flapping frequency. However, depending on various kinematic and dynamic system parameters, (i.e. flapping frequency, density ratio and pitching axis), the lateral induced velocity shows a number of different oscillating frequencies. Furthermore, compared with a one degree of freedom (DoF) wing in the lateral direction only, the propulsion performance of such a two DoF wing relies very much on the magnitude of torsional stiffness adding on the pivot point, as well as its pitching axis. In all cases examined here, thrust force and moment generated by a long span wing is larger than that of a short wing, which is remarkably linked to the strong reverse von Kármán vortex street formed in the wake of a wing.

Keywords: flapping wing, low aspect ratio, torsional spring

(Some figures may appear in colour only in the online journal)

1. Introduction

Micro air vehicle-motivated aerodynamics in biological flight has been an important subject in the past decade. Flying insects and birds, in general, perform remarkable flapping wing motion to create aerodynamic forces to stay airborne and for forward and darting flight. Flapping wing flight in natural flyers is a highly integrated field, which is both of interest to the MAV community and of importance to comparative morphologists when they are considering how physics constrains biological design (Shyy *et al* 2007).

There have been several series of developments on *flapping wing* studies. At the initial stage, research was focused on the generation of the wing's thrust force and propulsion efficiency via a *tethered wing* under a uniform incoming constant flow speed, e.g. the wing is limited

to a forced flapping motion without free movement in a forward/backward direction. For a comprehensive review of the research on various aspects of forced flapping wing, the reader is referred to the review papers Triantafyllou *et al* (2000), Liu (2005), Shyy *et al* (2007) and Liu *et al* (2010).

The assumption of a tethered flapping wing is obviously in contradiction to the live animal locomotion, where the thrust generation and propulsion direction is entirely determined by the complicated fluid force and the wing body dynamic interaction (Borazjani and Sotiropoulos 2009, Gazzola *et al* 2012).

Apart from the aforementioned limitation on tethered wings, most existing flapping wing study also assumes that the wing motion is immersed in a non-zero flow field with a uniform incoming flow velocity or Reynolds number. However, the examination on the development of the propulsion and maneuvering mechanism starting from a *zero-initial-velocity* has some practical applications, such as the sudden start process of swimming fish and hovering fliers. Under the zero-initial-velocity condition, the wing dynamic response to its flapping motion is also an ideal scenario for studying the *dynamic system instability development and bifurcation*.

In recent years, to understand flapping wing propulsion under the condition of free flight with a zero-initial-speed, some work has been devoted to the study of the dynamics of flapping wing with a *lateral* degree of freedom (DoF) (Vandenberghe *et al* 2004, 2006, Alben and Shelley 2005, Lu and Liao 2006, Zhang *et al* 2009 and Hu and Xiao 2013). In this context, the self-propelled fish swimming and flying birds with enforced vertical flapping motion is successfully modeled.

With a geometrically symmetric elliptic foil or a flat plate, the study on a symmetry-breaking bifurcation of a forced plunging foil or a plate is systematically examined either based on the experimental measurements (Vandenberghe *et al* 2004, 2006) or the numerical simulations (Alben and Shelley 2005, Lu and Liao 2006, Zhang *et al* 2009, and Hu and Xiao 2013). The general observation is that beyond a critical flapping frequency, Re_f, ($Re_f = \rho fac/\mu$, where f is flapping frequency, a is flapping amplitude, c is chord length, ρ and μ are density and viscosity of fluid respectively), the left–right symmetric flow structure around the foil with an up–down pure plunging motion will break, generating a net force in lateral direction, and thus leading to an in-line motion. Various hysteresis and bifurcations are observed depending on the different combinations of system kinematic and structural dynamic parameters, such as the flapping frequency, amplitude, foil density ratio and foil shape thickness etc. In order to observe the possible existences of diverse statuses, for example, a back-and-forth chaotic motion, a unidirectional forward or backward motion, a low flapping frequency and low density ratio foil is preferred. Therefore, in the above cited studies, the flapping frequency and density ratio are relatively low compared to real flyers, in the range of $Re_{\mathrm{fr}} = 0$–80 and density ratio of 0.2–20 (Alben and Shelley 2005, Zhang *et al* 2009 and Hu and Xiao 2013).

More recently, the study on the above mentioned flapping wing problem is developed one step further by taking into account the *wing system flexibility* (Spagnolie *et al* 2010, Zhang *et al* 2010, Kang and Shyy 2013 and Montcastle and Combes 2013). It is well known that a key feature in flapping wing flight or natural flyers' wings is their deformable structures that endure either a passively or actively variable shape, owing to their inertial and aerodynamic forces during flight. The aerodynamics and structural dynamics of such flapping wings are strongly coupled, which often leads to a complex fluid–structure interaction (FSI) problem. Therefore, it is of great importance to answer a central question of how the three-dimensional and passive change of wing kinematics due to inherent wing flexibility contributes to the unsteady aerodynamics and energetics in a flexible flapping wing flight (Nakata and Liu 2012).

To study the flapping wing system flexible impact on its propulsion performance, one common method utilized by some researchers is to introduce a torsional spring at its flapping pivot point (Spagnolie *et al* 2010, Zhang *et al* 2010). Previous studies by Combes and Daniel (2003a), (2003b) on the flexure stiffness variation of a hawkmoth and dragonfly observed that the flexibility decays sharply from the wing leading edge to the trailing edge and from the root to the tip. With the observation of high flexibility around the wing root, a *simplified structure dynamic model* to mimic the flexible role of large wings and appendage in the biologic flapping motion is to use a lumped-sum torsional flexibility model. In a context of free flying, the wing is free to move in the lateral direction, and is also able to pitch clockwise and anti-clockwise. The rotational motion is modeled by an elastic torsion spring acting on the pivot point (Ishihara *et al* 2009, Vanella *et al* 2009, Nakata and Liu 2012). By introducing these two DoFs both in the lateral and pitching directions, the biomimetic model is close to the nature flapping-based animal propulsive motions, where both the translation and pitching modes are passively induced.

A systematic numerical and experimental study on an elliptical wing with a forced heaving motion but passive pitching about its leading edge was performed by Spagnolie *et al* (2010). While the simulation was conducted at a much lower flapping frequency relative to their experiment ($Re_f = 10^5$ in experiment), many dynamic characteristics of wings are supported by their numerical results. Under the conditions of two mass ratio (M) defined as the mass of wing/mass of surrounding fluid ($M = 10$ and 1.0), non-dimensional flapping amplitude (A/c) of 0.5, dimensionless spring constant $k = 50\,000$ (torsional spring constant) and shape aspect ratio (AR) $e = b/a$ (thickness divided by chord length), increasing flapping Reynolds number (Re_{fr}), four flow regimes are found: (i) an almost left/right symmetric flow without lateral movement; (ii) an improved lateral motion with adding a torsional spring than without it (an increased net force in lateral direction); (iii) a deteriorated lateral performance relative to its rigid counterpart; (iv) a bi-stable status, hysteretic regime in which the flapping wing can move horizontally in either directions. Compared to a 1-DoF flapping wing in lateral free movement only, one significant finding is that a wing with 2-DoF including free-rotating could activate its lateral motion at a lower flapping frequency, clearly indicating that

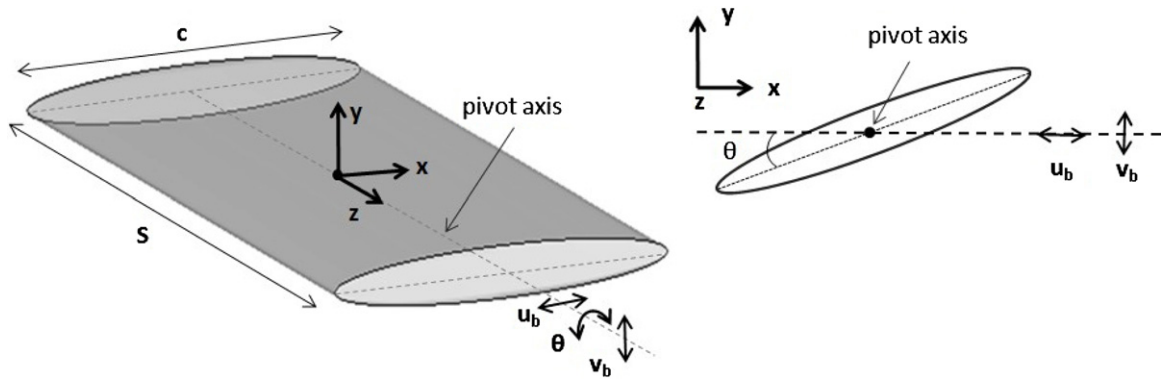

Figure 1. Sketch of the simulation model.

the system flexibility, represented by a pivot point torsional spring, is beneficial to the lateral thrust generation. In addition, the maximum lateral velocity is observed when the wing flaps at a frequency around system resonance frequency. The examination of the wing shape AR (e) varying from 0.1 to 1.0 also revealed a transition from coherent to chaotic motion and then a return to coherent motion when $e = 1.0$, where the wing becomes a circular cylinder.

The study addressing the role of the foil's stiffness has also been pursued by Zhang *et al* (2010) recently. Using a multi-block lattice Boltzmann method (LBM), a so-called flexible plate is modeled by a rigid plate with a torsional spring acting on the pivot point at the leading edge of the plate. They found that the dynamics response of foil presented a non-periodic status, a periodic forward status and periodic backward status by varying various foil kinematic and structure parameters. The exact boundaries between the above three regimes relied on the flapping amplitude as well as the wing linear density ratio (D) as well as frequency ratio (F), defined as the system natural frequency to the forced flapping frequency.

Except for the aforementioned two papers on 2-DoF flapping wings (Spagnolie *et al* 2010, Zhang *et al* 2010) no relevant research has been performed on a three-dimensional wing with relatively low ARs, i.e. AR $\leqslant$ 4.0 (AR is defined as span/chord length). Though a large AR assumption is valid for some animals with large fins, wings and appendages such as the wings of the tree sparrow, soaring birds and bumblebee, low AR fins/wings do exist, especially for fish pectorals. Previous studies on a low AR *tethered* wing found that the kinematic features of large ARs may be distinguished from that of low AR wings in terms of thrust and efficiency. The wake vortex topology also presented a remarkable three-dimensional effect which is strongly linked to the wing kinematic performance (Blondeaux *et al* 2005a, 2005b, Dong *et al* 2006). The question of whether the flow phenomena observed from a two-dimensional wing is applicable to a three-dimensional wing under a self-propelled 2-DoF condition is still open for investigation, and this paper provides new findings in this particular area.

In the present numerical study, we perform a comprehensive investigation on the dynamics response of a three-dimensional flapping wing with 2-DoF in lateral and rotational direction under a zero-initial-velocity condition. Our attention is mainly focused on the effect of wing ARs, flapping frequency (Re_{fr}), system torsional stiffness (represented by frequency ratio F), density ratio (denoted as σ, and defined as density of wing/density of surrounding fluid) and pitch-bias (x/c) on the development of system symmetry breakdown and the induced propulsion force, efficiency and related wake structure. The outline of the rest of the paper is as follows. We begin by describing the problem with relevant parameters that control the system kinematic and dynamics features along with the numerical approaches in section 2. In this section we also demonstrate the validity of the developed numerical methods in computing such flows. In section 3, a systematic presentation on the simulating results is included. We start with the examination on how the lateral and pitching movement of wing is activated by its vertical flapping motion, followed by a discussion on the results in the fully developed stable state. Distinguishing from the previous work, our particular interest is centered on the three-dimensional and pitch–pivot-point influence by comparison of the two-dimensional (AR $= \infty$) and three-dimensional (AR $\leqslant$ 4) wing data and bias pitching axis ($x/c \neq 0$) to bring out the difference between them.

2. Problem description and computational approach

2.1. The problem and numerical method

In this study, simulations are carried out for a three-dimensional rectangular wing (figure 1) under a forced plunging motion while with free motion in the lateral (x) and rotational (θ) direction. The wing has an elliptical cross-section and the ratio of thickness to chord length is 0.1, with the cross-sectional area (A_c) of 0.025 πc^2. The fluid motion is governed by a three-dimensional incompressible continuity and momentum equations:

$$\nabla \cdot \mathbf{u} = 0 \tag{1}$$

$$\frac{\partial \mathbf{u}}{\partial t} + \mathbf{u} \cdot \nabla \mathbf{u} = -\frac{1}{\rho}\nabla p + \frac{\mu}{\rho}\nabla^2 \mathbf{u} \tag{2}$$

where $\mathbf{u} = (u, v, w)$ is the fluid velocity, p is the pressure, μ the fluid viscosity and ρ is the fluid density.

A specified sinusoidal plunging motion is imposed on the wing, which is defined as

$$y_b = h \sin(2\pi f t) \tag{3}$$

where h is the flapping amplitude and f is the flapping frequency.

With two DoFs in the lateral and rotational directions, the wing movement in these two directions is solely determined by the fluid–motion coupling between the surrounded fluid and wing. The *induced* wing lateral motion in x direction is determined by Newton's second law as

$$m_b \frac{\mathrm{d}u_b}{\mathrm{d}t} = F_x \tag{4}$$

where u_b is the wing velocity in x direction, F_x is the x direction component of overall fluid force integrated around wing surface. m_b is the mass of wing ($m_b = SA_c\rho_b$, where S is the wing span-wise distance). For a two-dimensional wing, S is taken as one unit.

Induced wing rotational motion in θ direction is governed by a rotational momentum equation as based on a torsional spring assumption:

$$I\frac{d^2\theta}{\mathrm{d}t^2} + k\theta = M_z \tag{5}$$

where M_z is the fluid moment imposed on the wing, θ is the pitching angle, k is the spring stiffness, and I is the inertia moment of wing.

To determine the wing lateral location and velocity, an explicit time marching scheme is used to discretize equation (4) as

$${u_b}^t = \frac{F_x^{t-\Delta t}}{m_b}\Delta t + {u_b}^{t-\Delta t} \tag{6}$$

where ${u_b}^t$ and ${u_b}^{t-\Delta t}$ are the velocities at two subsequent instantaneous time of (t) and $(t-\Delta t)$, and Δt is the time step. The exact wing location is obtained by integrating equation (6) once.

The pitching angle (θ) is the solution of equation (5), where a fourth-order Runge–Kutta method is used:

$$\begin{aligned}
\dot{\theta}_{t_{n+1}} &= \dot{\theta}_{t_n} + \frac{\Delta t}{6}\cdot(K_1 + K_2 + 2K_3 + K_4)\\
K_1 &= \frac{M_z}{I} - \frac{k}{I}\cdot\theta_{t_n}\\
K_2 &= \frac{M_z}{I} - \frac{k}{I}\cdot\left(\theta_{t_n} + \frac{\Delta t}{2}\cdot\dot{\theta}_{t_n}\right)\\
K_3 &= \frac{M_z}{I} - \frac{k}{I}\cdot\left(\theta_{t_n} + \frac{\Delta t}{2}\cdot\dot{\theta}_{t_n} + \frac{(\Delta t)^2}{2}\cdot K_1\right)\\
K_4 &= \frac{M_z}{I} - \frac{k}{I}\cdot\left(\theta_{t_n} + \Delta t\cdot\dot{\theta}_{t_n} + \frac{(\Delta t)^2}{2}\cdot K_2\right)
\end{aligned} \tag{7}$$

where n represents the nth time step and $\theta_{t_{n+1}}$ and θ_{t_n} are the pitching angles at the instantaneous time of $(n+1)\Delta t$ and $n\Delta t$.

Flow field around the wing is simulated using the commercial CFD package FLUENT version 13.0, with an unsteady incompressible solver and the second-order upwind spatial discretization. The flow field is assumed to be laminar as the induced velocity between the wing and fluid is small with Re_u ranging from 0–1000 approximately. The first-order discretization is used for the unsteady time marching, which is limited by the DYNAMIC MESH function imbedded in FLUENT (ANSYS 2010). To avoid any inaccuracy that could be generated by the mesh deforming or re-meshing, the entire mesh domain is handled as a rigid moving body without relative *mesh motion* between the wing and the surrounding cells. A macro dealing with rigid motion (Define_CG_MOTION) written in User_Defined_Function is implemented on the entire domain.

At each time step, the simulation starts with attaining the flow field around wing by solving unsteady continuity and momentum equations associated with the velocity and pressure Dirichlet and Neumann boundary conditions. By obtaining the flow data, the integrated wing surface forces (F_x) and moment (M_z) in equations (4) and (5) are available. The dynamic response of wing is therefore obtained by solving equations (6) and (7) where the system structural parameters, such as the wing mass, stiffness are taken into account.

2.2. Parameter definition

The main kinematics and dynamic parameters are described in the following section. Wing AR is defined as the span-wise length (S, wing tip to tip distance) divided by chord length (c)

$$\mathrm{AR} = \frac{S}{c}, \tag{8}$$

where the chord length (c) is a constant.

To quantify the heaving frequency, the flapping frequency Reynolds number is defined as

$$Re_{\mathrm{fr}} = \frac{\rho h f c}{\mu}, \tag{9}$$

Obviously, Re_{fr} is an indication of the prescribed plunging frequency as the plunging amplitude (h) is fixed as $0.5c$.

Two non-dimensional parameters are relevant to the system dynamics response, i.e. density ratio (σ) and frequency ratio (F), they are defined as

$$\sigma = \frac{\rho_b}{\rho}, \tag{10}$$

and

$$F = \frac{f_n}{f}, \tag{11}$$

where ρ_b and ρ are the density of wing body and fluid surrounded it, respectively. f_n is the wing natural frequency, and defined as

$$f_n = \frac{1}{2\pi}\sqrt{\frac{k}{I}}, \tag{12}$$

where k and I are the stiffness of system and moment of inertia of the wing, respectively. The non-dimensional density ratio (σ) indicates the wing system inertia, and the frequency ratio (F) represents the rotational stiffness.

The overall parameters covered in the present study are summarized in table 1. Both the two-dimensional foil ($\mathrm{AR} = \infty$) and the three-dimensional wing with low AR ($\mathrm{AR} \leqslant 4.0$) are investigated. The frequency ratio (F) is mainly selected between 1.5 to 10.0 to control the wing dynamic response in rotational direction. Obviously, wing with F equal to infinity is the indication of one DoF in lateral (x) direction. The density ratio examined here is in-between 4.0 to 32. As compared to the relevant mass ratios for live flying birds or insects, such

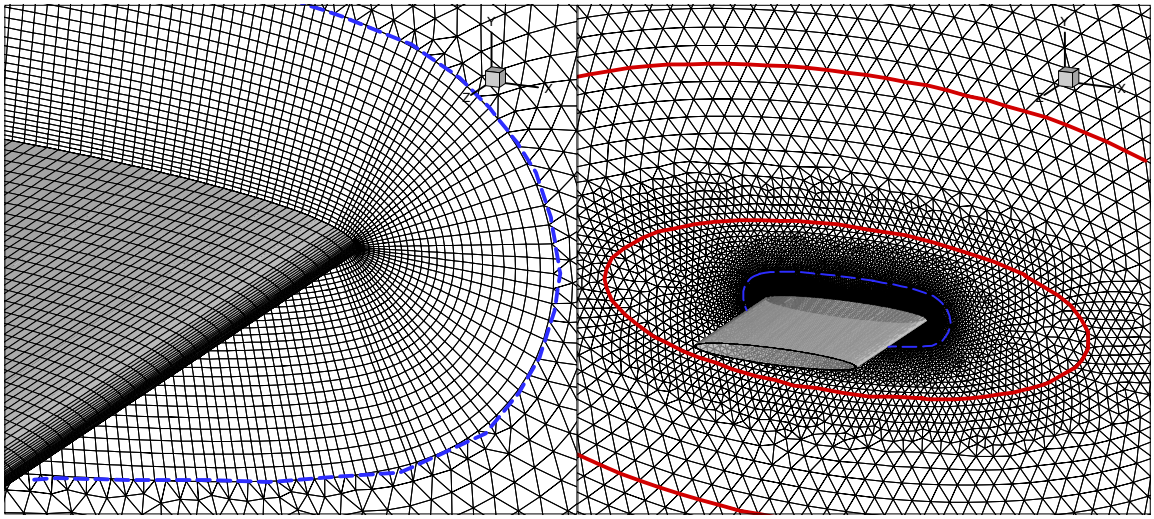

(*a*) (*b*)

Figure 2. Grid distributions over 3D wing. (*a*) Mesh around wing surface, a structured BL mesh is used near the wing. The blue circle represents the boundary of BL. (*b*) Overall mesh distribution. Mesh size progressively increases away from wing.

as the wings of hawkmoths, bumblebees and fruitflies, which are reported to be of 2.0×10^3, 2.1×10^3 and 1.1×10^3, respectively (Willmott and Ellington 1997a, 1997b, Combes and Daniel 2003a, 2003b, Buchwarld and Dudley 2010), the mass ratios studied here are very small.

In addition, the flapping Reynolds number $Re_{\rm fr}$ defined in equation (9), for the 3D wing in the present study, is fixed at 80, which is comparatively small as compared to the normal flapping wing cases in biological flights. However, since the main objective of the present study aims at unveiling the three-dimensional mechanisms in free-moving 3D wings with a specific focus on the phenomenon 'symmetry breakdown' and its subsequent development into stable states, the parameters selected are consistent with other relevant papers on free-moving two-dimensional foils by Alben and Shelley (2005) and a flat plate by Zhang *et al* (2010) with $Re_{\rm fr} = 0$–50 and $Re_{\rm fr} = 0$–80, respectively.

The wing pitching axis is initially set at the center of chord ($x/c = 0$ in figure 1) to hold the wing left/right and clockwise/counter clockwise symmetry before the bifurcation starts. This is different from the real flyers, where the rotational axis is normally at the leading edge (Sane and Dickinson 2002). As we will show later, the stiffness of wing, represented by frequency ratio F, on the induced lateral speed (Re_u) is remarkably affected by the pivot point. Thus, a systematic study is performed on the pitching axis effect by varying the pivot point from leading edge ($x/c = 0.5$) to center-chord ($x/c = 0$).

The computed data are summarized with the induced lateral non-dimensional velocity (Re_u) and the pitching angle ($\theta_{\rm rms}$) based on its root mean square value (rms), which is defined as

$$Re_u = \frac{\rho c|u_b|}{\mu}, \tag{13}$$

and

$$\theta_{\rm rms} = \sqrt{\frac{\sum_{r=1}^{i}(\theta^{t_r} - \theta_{\rm avg})^2}{i}}. \tag{14}$$

The i in equation (14) represents the iteration time step, $\theta^{\rm tr}$ is the pitching angle at the $r^{\rm st}$ instantaneous time, $\theta_{\rm avg}$ is the averaged pitching angle. As we will see in section 3, the wing eventually approaches a periodic pitch motion with a time–mean pitch angle always of zero, therefore, a rms expression of pitch angle is adopted herein.

The non-dimensional lateral and vertical overall force coefficient C_{Fx} and C_{Fy} are defined as

$$C_{Fx} = \frac{F_x}{0.5\rho(hf)^2cL}, \qquad C_{Fy} = \frac{F_y}{0.5\rho(hf)^2cL}. \tag{15}$$

The pressure force coefficient $C_{F_{P_x}}$ is represented by

$$C_{F_{P_x}} = \frac{F_{P_x}}{0.5\rho(hf)^2cL}. \tag{16}$$

The propulsion efficiency η is defined as

$$\eta = \frac{\int_t^{t+T} u_b(t)F_{P_x}\,{\rm d}t}{\int_t^{t+T} v_b(t)F_y\,{\rm d}t} \tag{17}$$

where F_x and F_y are the force components in lateral and vertical direction, F_{P_x} is pressure force in the lateral direction, and L is a characteristic length assuming one unit herein.

2.3. Sensitivity study and validation

The mesh distribution over the 3D wing is shown in figure 2. A structured boundary layer (BL) mesh is used for the flow near wing surface, with 25 layers in total within BL. For the grid outside the BL area, a triangular mesh is used.

A grid and time-step independence test is conducted for a 3D wing with AR of 1.5 under $Re_{\rm fr} = 60$, $F = \infty$ and $h/c = 0.5$ conditions. Details of overall volume and surface mesh numbers and time step are listed in table 2 along with the computed approach velocity U_b/fc. The instantaneous C_{Fx} *on* the medium and fine grids (not shown here) indicate that the results on the medium grid with a time step of ${\rm d}t = T/200$ almost coincide with those on the fine grid and ${\rm d}t = T/400$. Considering an increased computing time as listed in table 2,

Table 1. Various parameters investigated in the present study.

Density ratio σ	Plunging amplitude (h/c)	Flapping Re (Re_{fr})	Frequency ratio (F)	Aspect ratio ratio (AR)	Pitching axis position (x/c)
4–10, 16	0.5	80	1.5–10	1.0,1.5, 2.0,3.0, 4.0	0
4–10, 16	0.5	80	1.5–10	∞	0, 0.1, 0.2, 0.3, 0.4, 0.5
4, 20, 32	0.5	20, 32, 45, 60, 80	∞	1.0,1.5, 2.0,4.0, 6.0, ∞	–

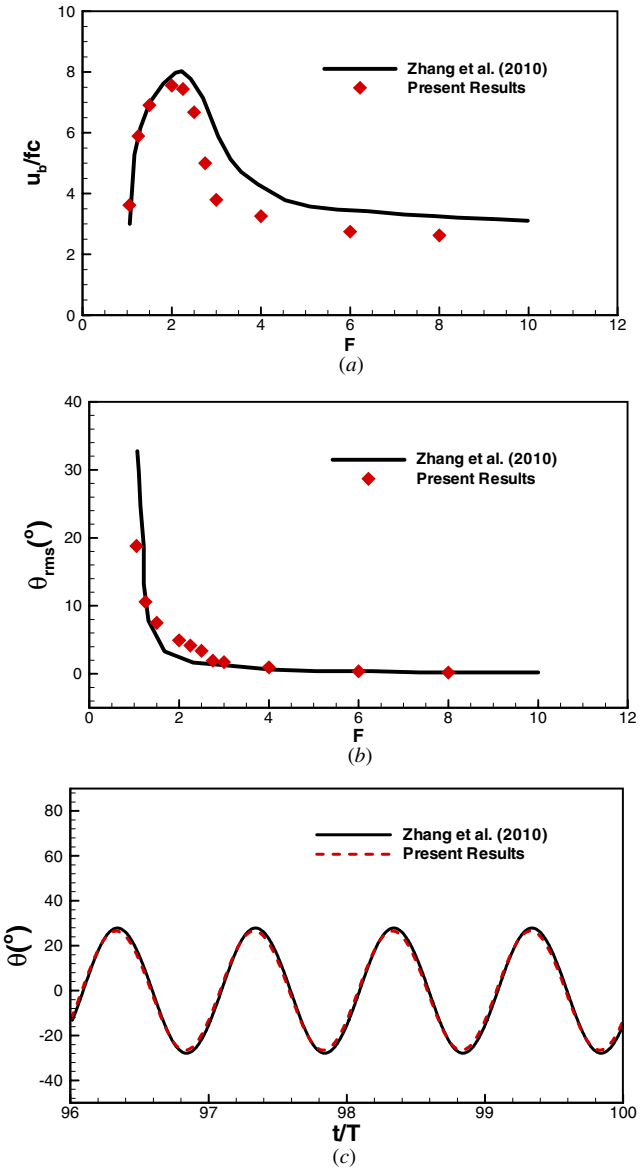

Figure 3. Comparison with Zhang *et al* (2010) with 2-DoF flat plate. (*a*) Induced non-dimensional lateral velocity. (*b*) Induced pitching angle. (*c*) Variation of induced instantaneous pitching angle at $F = 1.05$.

the time step d$t = T/200$ and medium mesh is used in the present simulation.

The numerical methodology developed for solving the problems with unsteady forced undulating swimming fish or two-dimensional flapping foil has been extensively validated in our previous publication (Hu *et al* 2011 and Xiao *et al* 2011). To further validate the strategy utilized to handle the system dynamic response (FSI) associated with the self-propelled feature, a validation on a self-propelled flat plate investigated by Zhang *et al* (2010) is performed. Given the pre-specified plunging motion with a flapping $Re_{\mathrm{fr}} = 40$, amplitude $h/c = 0.5$ and mass ratio $\sigma_l = 2.0$, the computed propulsion velocity (Re_u) and pitching angle (θ) variation with frequency ratio are compared in figure 3 with data from Zhang *et al* (2010). Our results present a general good agreement with theirs by capturing the peak Re_u and sharp varying of Re_u and θ versus F. At large F, we have discrepancy as compared to Zhang *et al* (2010), this might be caused by the different numerical methods used. A multi-block LBM was applied by Zhang *et al* (2010), while our method is based on a finite volume method. In addition, due to the limitation of the present method, we could not get convergent solution for $F \leqslant 1.0$. However, the comparison on the time-dependent instantaneous pitching angle at $F = 1.05$ presents an excellent agreement between two results in terms of the amplitude and phase angle. Apart from this test case, we also simulated a two-dimensional flapping elliptic foil which was studied previously by Alben and Shelley (2005). The comparison between our results and theirs is published in our recent paper (Hu and Xiao 2013).

3. Results and discussions

In this section, we start presenting our results on a symmetry breakdown which leads to the wing motion in both rotational and lateral direction in subsection 3.1. The results on the fully developed stable state are discussed in subsections 3.2, 3.3 and 3.4. Section 3.2 focuses on our findings of a complicated flow status map obtained by subjecting the wing to a wide range of kinematic and system dynamic parameters. This will be followed by a detailed parametric study on the wing AR, pivot point, density and frequency ratio influence on the flow structure, the system dynamics response in terms of the instantaneous, final approaching propulsion velocity, rotational angle, thrust force and efficiency.

3.1. Symmetry breakdown

The observations on the evolution of wing up and down heaving motion show that, given the forced $Re_{\mathrm{fr}} = 80$, the wing under various grouping of ARs, density ratios, frequency ratios and pitching bias distance could eventually reach a stable motion, a combination of an either forward or backward motion with a periodic pitching motion. The evolution of instantaneous Re_u and θ are shown in figures 4 and 5 for two-dimensional foil (AR $= \infty$) and three-dimensional wing (AR $= 2$). It is clear that the wing starts its lateral movement

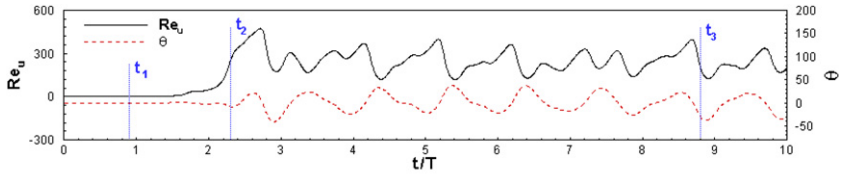

(*a*) Instantaneous Re_u and θ

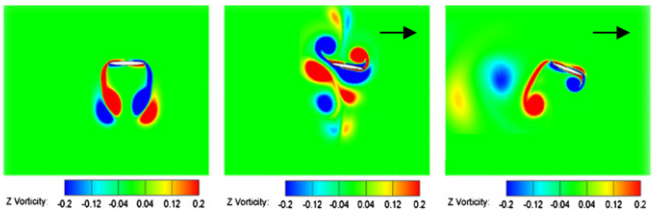

(*b*-i) t_1=0.9T (*b*-j) t_2=2.3T (*b*-k) t_3=8.8T

Figure 4. Evolution of symmetry breakdown ($\sigma = 8.0$, $Re_{\rm fr} = 80$, $F = 2.0$, AR $= \infty$). (*a*) Instantaneous Re_u and θ. $z/S = 0$ (*b*-i) $t_1 = 0.9T$. (*b*-j) $t_2 = 4.9T$. (*b*-k) $t_3 = 9.9T$. $z/S = 0.25$ (*c*-i) $t_1 = 0.9T$. (*c*-j) $t_2 = 4.9T$. (*c*-k) $t_3 = 9.9T$. $z/S = 0.5$ (*d*-i) $t_1 = 0.9T$ (*d*-j) $t_2 = 4.9T$ (*d*-k) $t_3 = 9.9T$.

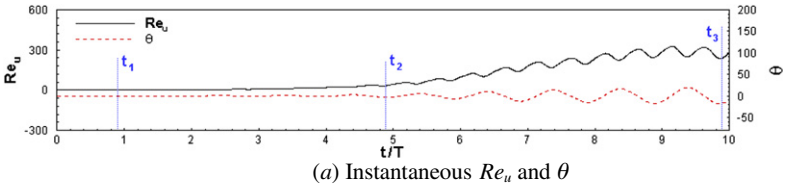

(*a*) Instantaneous Re_u and θ

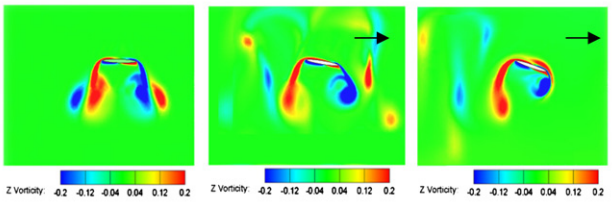

z/S=0 (*b*-i) t_1=0.9T (*b*-j) t_2=4.9T (*b*-k) t_3=9.9T

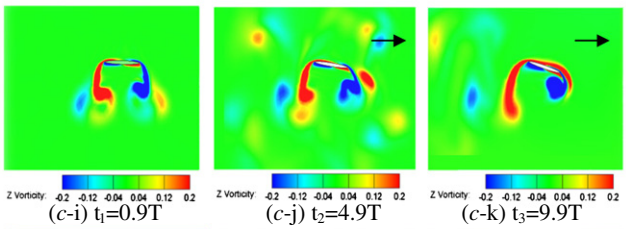

z/S=0.25 (*c*-i) t_1=0.9T (*c*-j) t_2=4.9T (*c*-k) t_3=9.9T

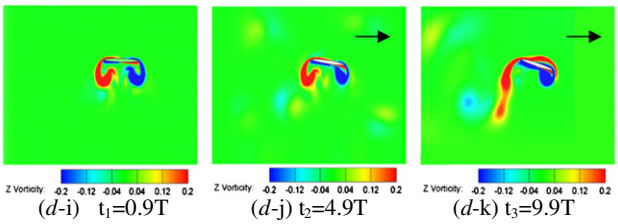

z/S=0.5 (*d*-i) t_1=0.9T (*d*-j) t_2=4.9T (*d*-k) t_3=9.9T

Figure 5. Evolution of symmetry breakdown ($\sigma = 8.0$, $Re_{\rm fr} = 80$, $F = 2.0$, AR $= 2.0$). (The contour legend is same as in figure 4.)

Table 2. Summary on mesh size, time step and computing time.

Mesh	Overall cells	Nodes (wing surface)	Nodes (span-wise)	Time step	Simulation time (eight processors)	U_b/fc
AR1.5-C	185 3675	200	80	$T/200$	59 h	4.37
AR1.5-M	278 2250	300	80	$T/200$	75 h	3.95
AR1.5-F	632 7830	400	120	$T/200$	153 h	3.91
AR1.5-MST	278 2250	300	80	$T/150$	62 h	4.24
AR1.5-MLT	278 2250	300	80	$T/400$	140 h	3.96

C: coarse mesh; M: medium mesh; F: fine mesh; MST: medium mesh and small time step; MLT: medium mesh and large time step.

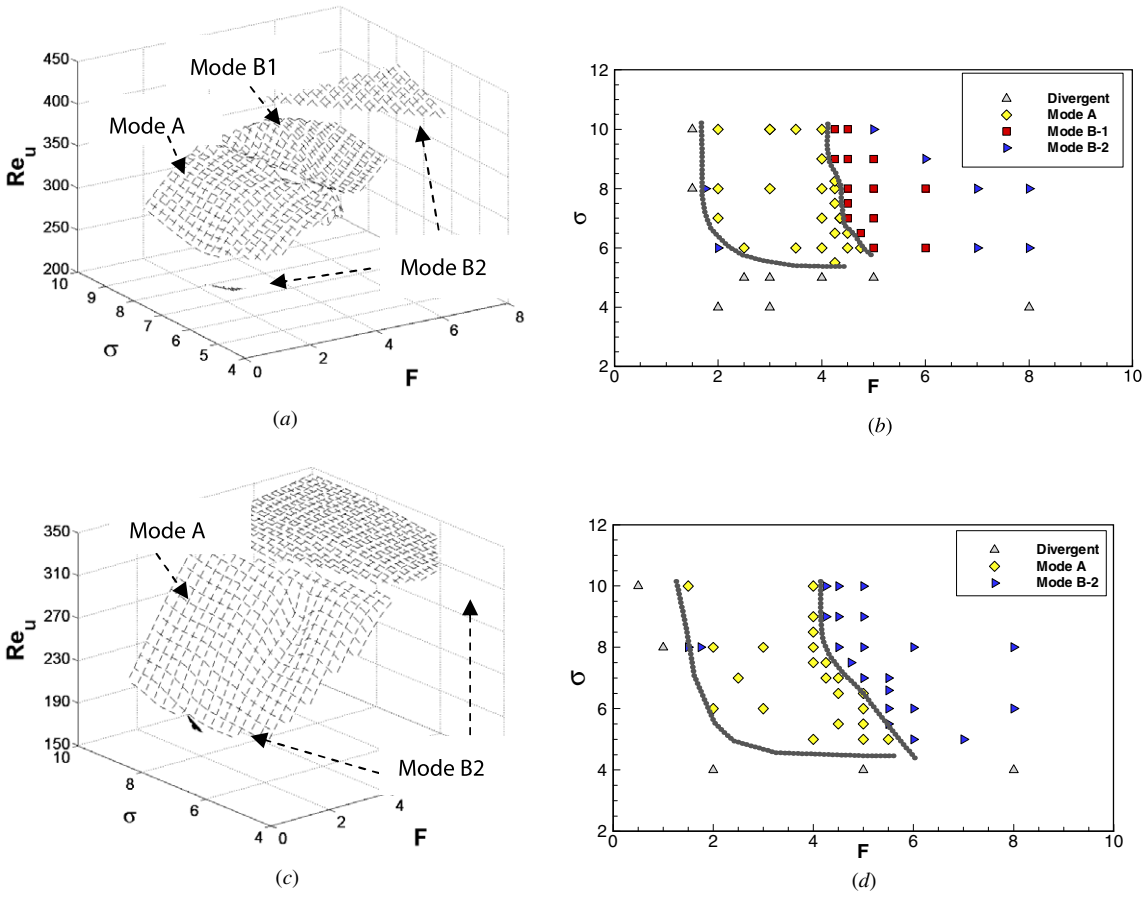

Figure 6. Boundary of various flow status ($h/c = 0.5$, $Re_{\mathrm{fr}} = 80$). (*a*) Density–frequency ratio-Re_u three-dimensional view (AR $= \infty$). (*b*) Density-frequency ratio plane view (AR $= \infty$). (*c*) Density–frequency ratio-Re_u three-dimensional view (AR $= 2.0$). (*d*) Density-frequency ratio plane view (AR $= 2.0$). Mode A represents the state with multiple peak frequency obtained by FFT analysis on Re_u-time curve. Mode B-1 refers to the state with one dominant frequency which is equal to the forced plunging frequency. Mode B-2 depicts the state with one peak frequency which is double the forced plunging frequency.

almost at the same time as its rotational motion, indicating that once the pitching motion is activated, left/right symmetry breaks down and thus causes the lateral motion. A three-dimensional wing takes longer developing time than a two-dimensional foil to reach its stable state.

To better understand the wing dynamic system symmetry breakdown, the vorticity contours at three typical time instants, i.e. symmetry, asymmetry development and fully developed state (denoted as t_1, t_2 and t_3, respectively) are plotted in figures 4 and 5. Clearly seen from the plots, at time t_1, the flow structure has left/right symmetry, thus no movement of the wing in lateral and rotational directixons (figures 4(*b*-i), 5(*b*-i)–(*d*-i)). Once the wing flaps more cycles to reach time t_2, the pitching motion activates, as shown in figures 4(*b*-j) and 5(*b*-j)–(*d*-j), with an asymmetry vortex structure around the wing. At the fully developed state (t_3), a thrust-generated vortex wake is observed from figures 4(*b*-k) and 5(*b*-k)–(*d*-k). Comparison of figure 5(i) with (j) and (k) on the vortex structure around the wing at different span (z), reveals that the flow has a profound three-dimensional feature due to the low AR of the wing (AR $= 2$). A comparison between the 3D wing symmetry plane vorticity contour plot with a 2D wing in figures 4 and 5 also indicates a relatively weak vortex strength associated with a 3D wing, implying a weaker propulsion feature wake structure which is the key reason leading to a smaller Re_u and θ as compared to their 2D counterparts, which is shown later in the paper.

3.2. Various flow status at a fully developed state

Figures 6(*a*)–(*d*) are the charts (σ–F–Re_u and σ–F plane) summarizing the different flow status obtained with a 2D and 3D wing response (AR $= 2.0$), respectively. Each point in the chart represents simulated data obtained after a periodic stable status has been reached. For completeness, some points at the left margin in figures 6(*b*) and (*d*) represent the status where a convergent solution is not reachable. The corresponding time history on the instantaneous Re_u and θ, their power spectral density (PSD) distribution, and vorticity topology contour are shown in figures 7 and 8 with a range of frequency ratios varying from $F = 3.0$ to $F = 8.0$.

Our general observations are that the wing response in rotational direction (θ) to the forced flapping motion is generally more regular than the response in lateral direction. The fast Fourier transformation (FFT) analysis on the instantaneous θ plot, shown in figures 7 and 8, dictate that one

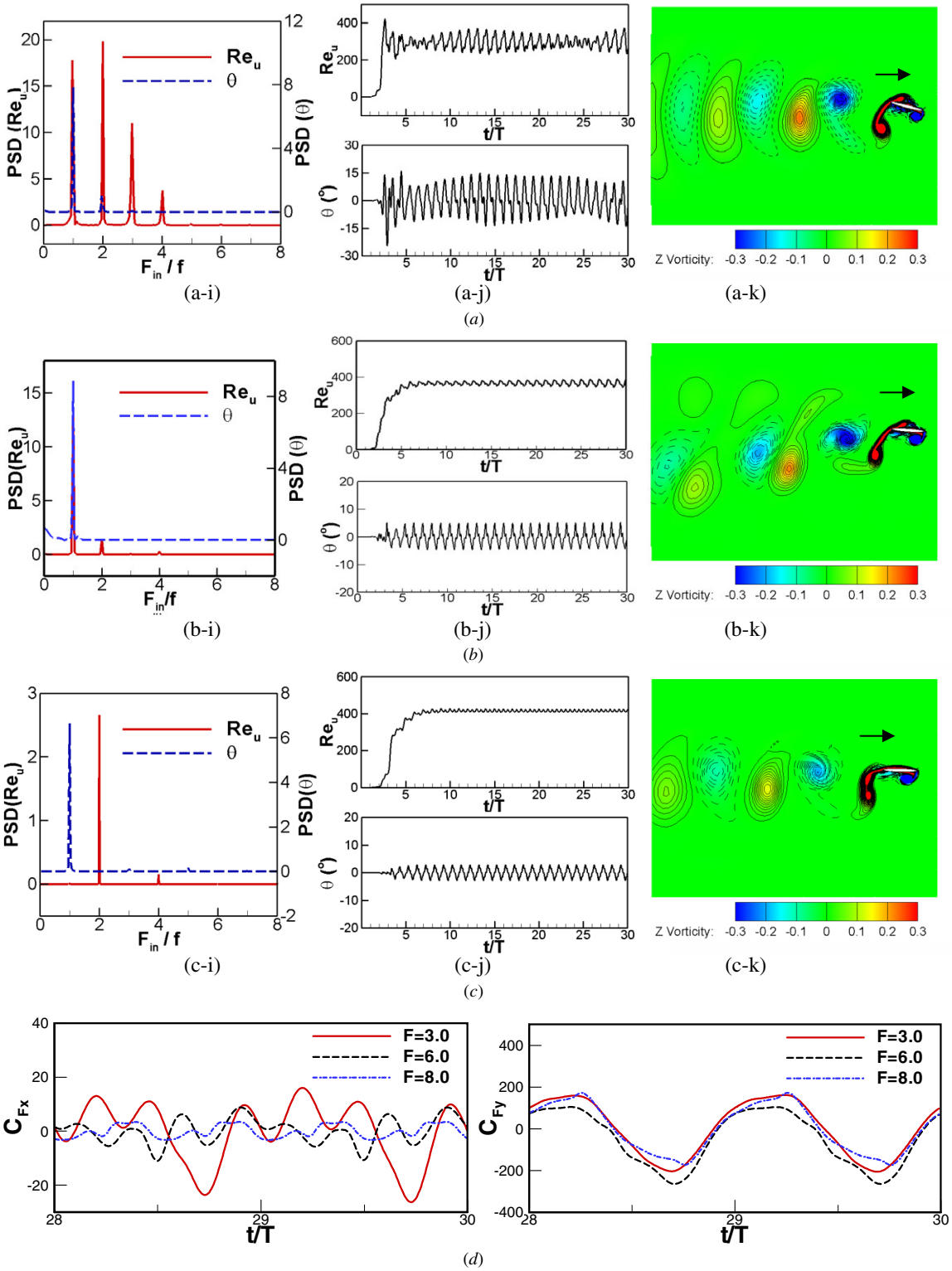

Figure 7. Evolution of instantaneous Re_{fr} and θ, their PSD, vorticity contour, and forces ($\sigma = 8.0$, $h/c = 0.5$, $Re_{\mathrm{fr}} = 80$ and AR $= \infty$). For vorticity contour, solid lines are positive values and dashed lines are negative values. (*a*) Mode A ($F = 3.0$). (*b*) Mode B-1 ($F = 6.0$). (*c*) Mode B-2 ($F = 8.0$). (*d*) Instantaneous thrust and lift forces.

dominant frequency, i.e., a single spike is always observed for all cases studied, which is identical to the flapping frequency (i.e. $F_{\mathrm{in}}/f = 1$, where F_{in} is the induced lateral motion frequency and f is the prescribed plunging frequency). The FFT is calculated from 10th period to 30th period. For some 2D wing at a low frequency ratio where F is less than 4.5, a second spike or more is observable. This is consistent with our system dynamic feature where the stiffness is imposed merely in the rotational direction to manipulate the periodic pitching motion, as shown in equation (5). In contrast, the FFT on

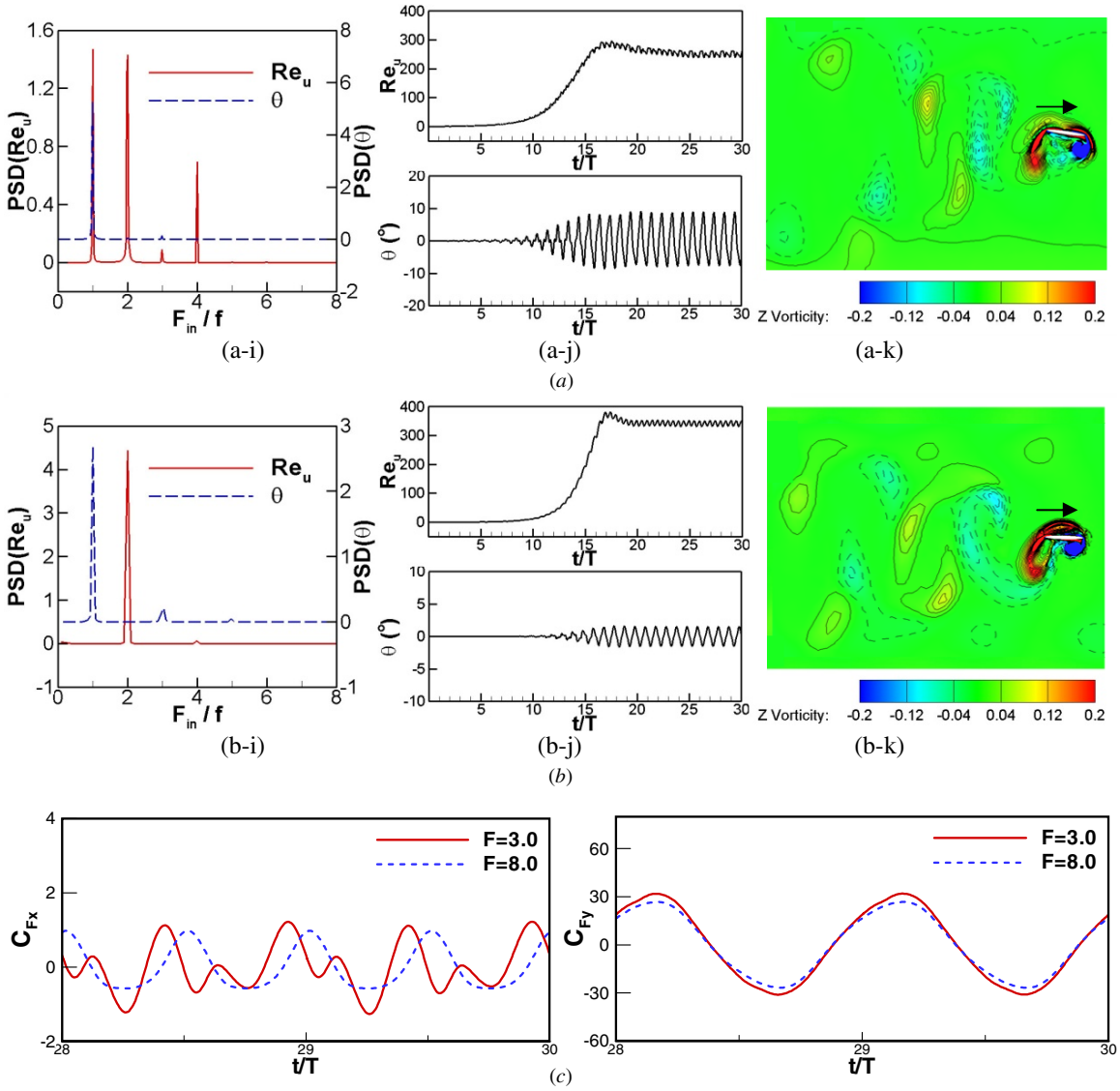

Figure 8. Evolution of instantaneous Re_{fr} and θ, their PSD and vorticity contour ($\sigma = 8.0$, $h = 0.5$, $Re_{\mathrm{fr}} = 80$ and AR $= 2.0$). For vorticity contour, solid lines are positive values and dashed lines are negative values. (*a*) Mode A ($F = 3.0$). (*b*) Mode B-2 ($F = 8$). (*c*) Instantaneous thrust and lift forces.

the instantaneous Re_u, history, which represents the dynamic response in lateral direction, reveal a multiple-spike frequency spectral distribution, where the dominant spike does not always correspond to the forced flapping frequency. Instead, it depends on a wide range of density and frequency ratio investigated. In the following, we classify such complicated flow status based on the FFT analysis on the instantaneous induced Re_u three ways.

- **Frequency ratio**: with an increase in frequency ratio (F) or wing stiffness, the PSD for Re_u shows a gradual transition from a multiple-spike (two–three modes) state to the single spike frequency state (one mode). We denote the state exhibiting multiple-spike frequency as mode A, and the state with single spike frequency as mode B. Two subdivisions as mode B-1 and B-2 are further defined depending on whether the F_{in}/f is equal to 1.0 or 2.0. It is found that the boundary between mode A and B is affected by the system dynamics parameters, i.e. density and frequency ratio. Given a fixed density ratio, the wing with large F presents a more harmonic distribution in terms of Re_u versus time plot, indicating the existence of one dominant frequency. This is also well reinforced by the instantaneous thrust and lift forces (C_{Fx} and C_{Fy}) plots in figures 7(*d*) and 8(*c*). Clearly seen, the lift force presents a rather regular dominant frequency, which is irrelevant to the stiffness (F). However, thrust force displays an increased multiple mode with small stiffness, which is believed to cause the multiple frequency in Re_u. From this point, the present results clearly reveal that the torsional stiffness, represented by the spring added at pivot point, definitely plays a role in the overall wing dynamic response both in x and θ direction. With F approaching infinity, the pitching motion is entirely eliminated, the wing becomes a rigid body with 1-DoF in x direction, and thus it is expected to be more stable and regular under the

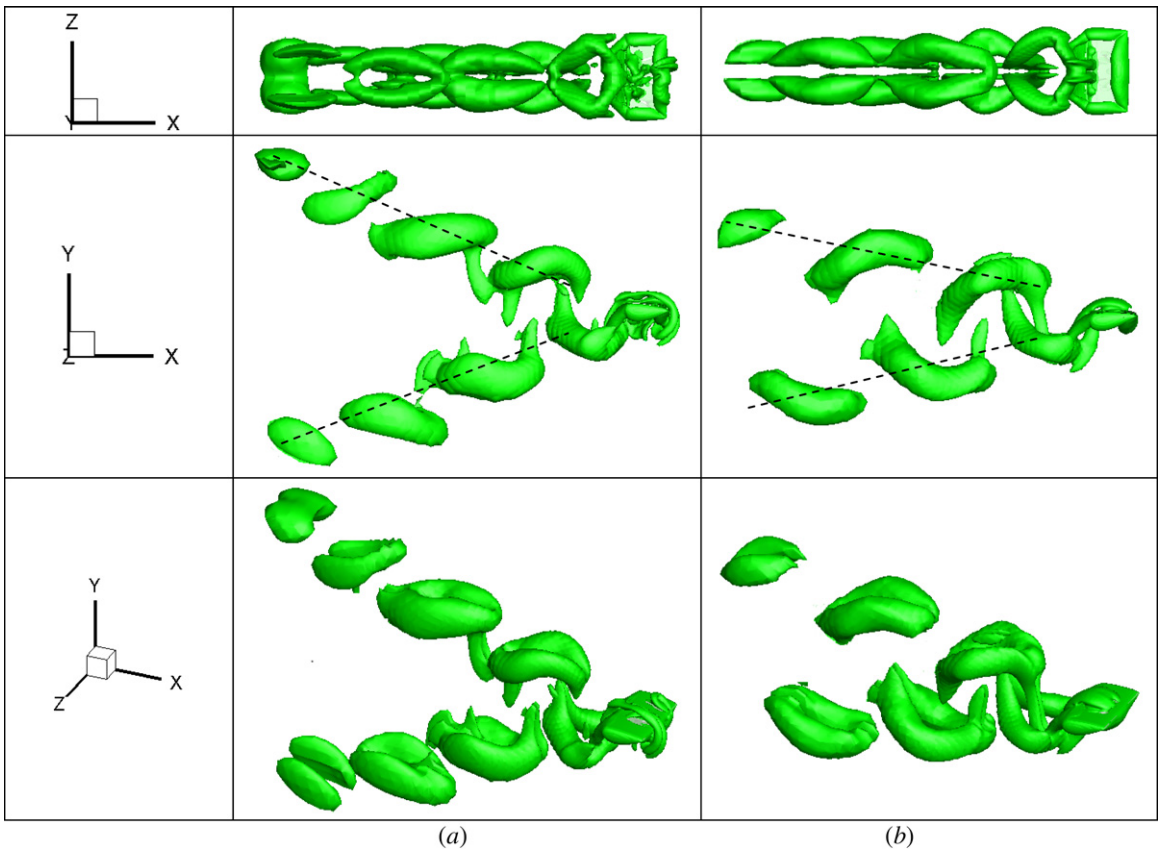

Figure 9. Vortex topology (Q contour) for 3D wing at different frequency ratios, with magnitude of iso-surfaces as 0.0002 (($\sigma = 8.0$, $h = 0.5$, $Re_{\mathrm{fr}} = 80$ and AR $= 2.0$)). (*a*) $F = 3.0$. (*b*) $F = 8.0$.

external forced flapping motion. Indeed, we found that only one peak frequency exists in its PSD.

- **Aspect ratio**: the wing AR influences the boundary separating mode A and B slightly. Decreasing AR leads to the boundary moving to higher F. Apart from that, AR also changes the mode transition and the ratio of the induced Re_u frequency relative to flapping frequency (F_{in}/f). Comparing 2D wing in figures 6(*a*) and (*b*) with 3D wing in 6(*c*) and (*d*), it can be seen that an increase in F causes a 3D wing to transfer from mode A directly to mode B-2.
- **Density ratio**: above trends are valid for all density ratios investigated. However, the exact boundary location is affected by density ratio (σ). In fact, decreasing density ratio causes the flow regime transition from mode A to B at a relatively large frequency ratio (F).

Along with the key information provided by FFT analysis above, the typical vorticity topology contours at a given density ratio $\sigma = 8.0$ are shown in figures 7 and 8 to represent the relevant wake vorticity structure variation with a gradually increasing F from mode A to B-1 to B-2. All vorticity plots shown in the figures are taken at the instantaneous time at which the wing pitches to the maximum angle. For a 3D wing, the vorticity contour is taken at wing half span section. It is seen that the vortical structure resembles the classic reverse von Kármán vortex street in the wake of a propulsive body, revealing the existence of a forward moving state. This behavior is consistent with the experimental and numerical findings of a 2D foil in the work of previous studies (Vandenberghe *et al* 2004, 2006, Alben and Shelley 2005, Lu and Liao 2006, Zhang *et al* 2009). However, some differences do exist. For a small frequency ratio (F), a less stiff wing with the presence of mode A, the pitching angle is relatively larger as compared to that of large F, where mode B appears, the vortex shedding street becomes much wider, and more vortices shed within one cycle, which leads to the co-existing of various PSD modes in the wake as shown previously. Increasing F causes the increasing of system stiffness and thus the wing pitching at a smaller angle. As a consequence, the wake becomes narrower and more regular, and fewer vortices shed in one cycle as compared to the cases with small F. Though the above observation is generally true for both 2D and 3D wings, the detailed difference can be noticed from the 3D wing wake topology plotted using a Q-criterion theory (Hunt *et al* 1988) as shown in figure 9. At a low AR, like AR $=$ 2.0, a vortex ring forms via the combination of two tip vortices generating at the two ends of wing-span direction.

3.3. Aspect ratio, frequency ratio (flexibility) and pivot-point effect

In this section, our attention is paid to the impact of variables AR and F and pitching axis on the development of Re_u, θ

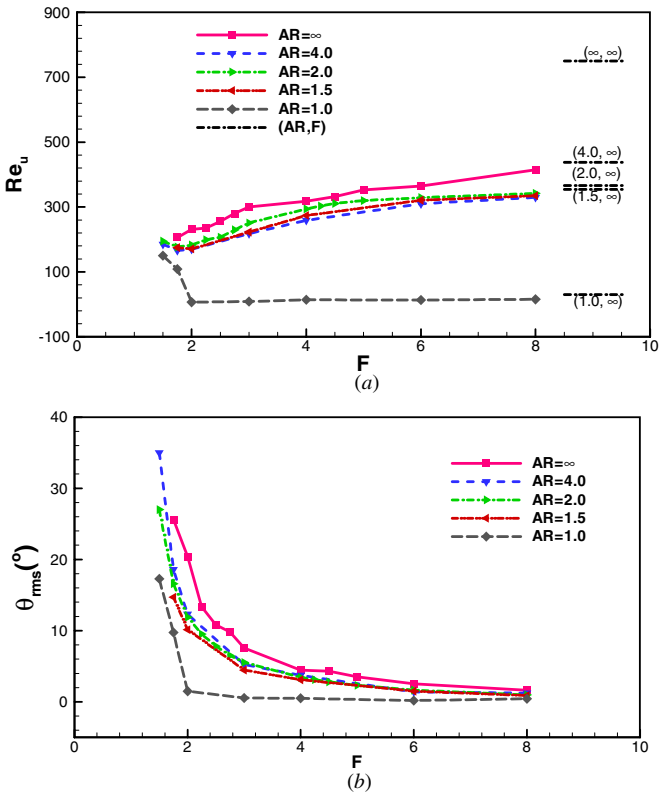

Figure 10. Final approached time-mean Re_u and $\theta_{\rm rms}$ ($\sigma = 8.0$, $Re_{\rm fr} = 80$, $x/c = 0$). (*a*) Induced non-dimensional lateral velocity. (*b*) Induced pitching angle.

and their quasi-periodic values. Figures 10(*a*) and (*b*) show the induced time-averaged lateral velocity (Re_u) and the rms pitching angle ($\theta_{\rm rms}$) variation with frequency ratio (F) at various ARs. At a predefined value of AR with 1-DoF in x-direction ($F = \infty$), the results are compared with the 2-DoF situations in figure 10(*a*).

For a moderate AR (ranging from 2.0 to 4.0) and a large F ($F > 4.0$), the differences in Re_u and $\theta_{\rm rms}$ are small. However, it is observed that a 2D wing (AR $= \infty$) obviously has larger propulsion velocity and pitching angle than those in a 3D wing. The impact of AR becomes more evident when the 3D wing becomes very short at AR $= 1.0$, where both lateral and rotational motions are remarkably independent on the frequency ratio F, different from the trend observed for AR $\geqslant 1.5$.

As for the stiffness effect, generally, a stiffer wing with larger frequency ratio tends to have a decreased pitching angle. Within the F ranging from 1.5 to 3.0, the pitching angle decays rapidly, and approaches almost zero around $F = 8.0$. This is consistent with the fundamental principles of frequency ratio. In fact, the case with $F = 1.0$ corresponds to a special condition where the flapping frequency is exactly equal to the wing's natural frequency. Recent studies by Kang *et al* (2011), Ramananarivo *et al* (2011) etc on the biological flights associated with insects/birds, reported that the maximum propulsive force is obtained when the wing flaps near its resonance frequency, whereas the optimal propulsive efficiency is reachable when the wing flaps at about half of its natural frequency. This implies that the propulsion performance of a flapping wing very likely demonstrates its apparent dependence on the forced flapping frequency, in particular at a low F, i.e. less than 4.0 as illustrated in figure 10, where the flexibility plays a significant role. Even though the current setup is away from the range of biological wings, such as some parameters' space setting and the utilization of a lumped elasticity of wing represented by an elastic spring at the pivot point, a similar phenomenon to the findings of Kang *et al* (2011) and Ramananarivo *et al* (2011) are observed. This suggested that the current model could be served as a good approximation for investigating flexible wing with passive pitch problems.

One striking finding from figure 10 is that, apart from a very low AR case with AR $= 1.0$, the lateral Re_u increases monotonically with frequency ratio of the wing for the rest of AR examined. This implies that the performance of a wing with torsional spring is even worse than a wing without spring, which seems contradictory to the study of Spagnolie *et al* (2010) and Zhang *et al* (2010). To find out the problem, we performed a series of investigation on the pivot point effect by varying it from center-chord ($x/c = 0$) to leading edge ($x/c = 0.5$). The results are presented in figure 11 for 2D and 3D wings. Clearly found from the plots, the pivot point has a very apparent impact on the stiffness influence for wing propulsion. Our two-dimensional results plotted in figures 11(*a*) and (*c*) clearly show that below a threshold pitching axis, $x/c = 0.3$ here, a wing without torsional spring achieves a better propulsion performance than a wing with spring. Beyond this value, Re_u versus F curve presents a non-monotonical trend. At a low F less than 2.0, where the wing is very flexible in rotational direction, the wing propulsion velocity increases sharply with F, exhibiting a flexible detrimental effect. Once F is larger than 2.0, Re_u decreases with F, thus indicating a better performance of a flexible wing than a rigid wing. The induced pitching angles decreases with the increase of F. Our results for $x/c > 0.3$ are remarkably similar to all relevant flexible wing flapping observations where the pitching axis is fixed at the leading edge (Spagnolie *et al* 2010, Zhang *et al* 2010). Another notable feature observed from figure 11 is that such pitching axis influence decays when the wing becomes more and more stiff (via increasing F), and is expected to lose its impact eventually when the wing turns into rigid.

To further demonstrate the above facts from the present study, the time-mean thrust pressure force ($C_{F_{Px}}$) in the lateral (x) direction and the corresponding propulsion efficiency η defined in equations (16) and (17) are plotted in figures 12(*a*) and (*b*) with various frequency ratios (F) and ARs. Obviously seen from the plots, the thrust force decreases monotonically with F for all ARs examined. The maximum $C_{F_{Px}}$ reaches at the minimum frequency ratio at around $F = 1.5$ studied. However, an optimal efficiency is obtained around $F = 2.0$ and $F = 3.0$ for 2D foil and 3D wing, respectively. This definitely reinforces the optimal propulsion mechanism in the field of biology as revealed by relevant publications cited above (Kang *et al* 2011, Ramananarivo *et al* 2011). Refer to the flow status results presented in section 3.2, we can conclude that the most desirable and efficient propulsion mode is mode A. Compared

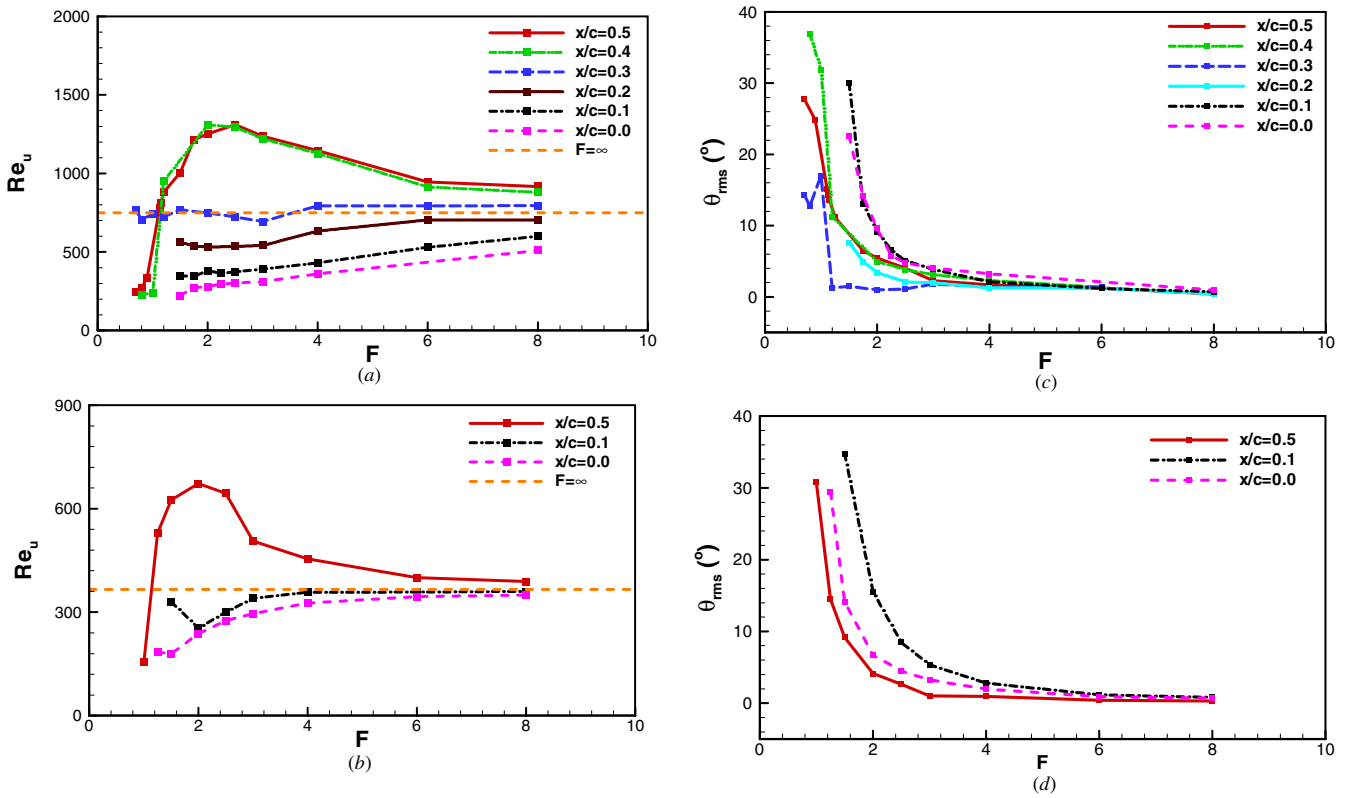

Figure 11. Effect of pitching axis ($x/c = 0$ represents the wing pitching at its center-chord). (*a*) Re_u versus F with AR $= \infty$. (*b*) Re_u versus F with AR $= 2.0$. (*c*) $\theta_{\rm rms}$ versus F with AR $= \infty$. (*d*) $\theta_{\rm rms}$ versus F with AR $= 2.0$.

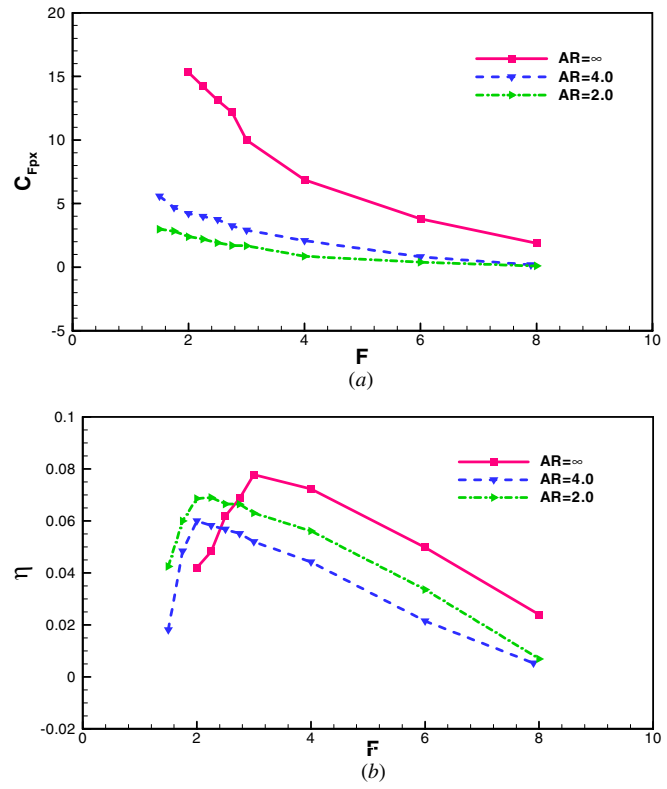

Figure 12. Frequency ratio (F) effect on the horizontal thrust force and efficiency ($\sigma = 8.0$, $Re_{\rm fr} = 80$). (*a*) Thrust force coefficient. (*b*) Efficiency.

to live fliers, the relative low efficiency shown in figure 12(*b*) might be due to the discrepancy in the selecting of problem parameters, such as flapping frequency ($Re_{\rm fr}$) and density ratio (σ), which are different from the real animals as we mentioned in section 2.

3.4. Density ratio effect

The results for density ratio (σ) effect on time-mean Re_u and θ are summarized in figures 13(*a*) and (*b*) for various ARs and frequency ratios (F). Generally, the impact of density ratio on the lateral velocity Re_u is smaller than its influence on θ. In addition, the density ratio impact is influenced by the wing AR. For a 2D wing under 2-DoF, represented by (∞, *) in the figure, increasing density ratio leads to a slightly enlarged Re_u and a small pitching angle. This trend is also relevant to wing stiffness (F). Large F implies a much stiffer wing, thus the density ratio effect is less apparent. This is clearly reflected by the wing with a (∞, ∞) combination, where the pitching angle is equal to zero and thus Re_u remains a constant as 755. With a 3D wing, given a density ratio (σ), again, we found that large AR has a relatively large propulsive velocity and rotational angle. For the present problem, i.e. a self-propelled 3D wing with 2-DoF, this finding is especially important, as it links the system dynamic response to the external fluid force. In particular, the inertial force influence on the system stability via the density ratio. With a fixed density ratio, the mass of a small AR wing must be smaller than a wing with large AR. The small mass represents a system with small inertia, and thus

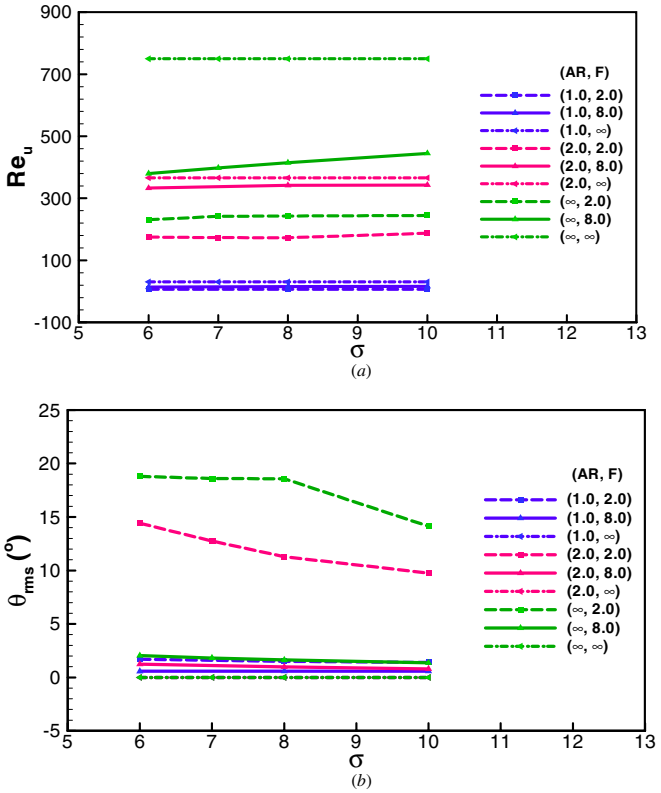

Figure 13. Density ratio effect on the induced lateral velocity and pitching angle ($Re_{\rm fr} = 80$). (*a*) Averaged induced non-dimensional lateral velocity $Re_{u.}$ (*b*) Induced pitching angle θ.

more sensible to the variation given from the external force or moment.

The development history of Re_u and θ are plotted in figure 14 for various density ratios at AR = 2.0 and F = 2.0. Obviously seen, due to the larger inertia, the system with large density ratio presents a small variation both on Re_u and θ. The evolution time to reach the final stable state is also increased. It should be pointed out that the wings of insects and birds usually have much larger density ratios on the order of several thousands (Ramananarivo *et al* 2011), which compared to the relatively low density ratios in the present study, may enhance the stability of the dynamic flight system in terms of the nonlinear interaction between aerodynamics and inertial dynamics.

4. Conclusions

A numerical study is carried out to investigate the dynamics of a three-dimensional low AR wing that flaps up and down but the pitching and horizontal motions are passively induced. The wing system stiffness is introduced and modeled by a torsional spring at the pivot point. The present study aims to understand the fundamental fluid mechanism utilized by some live animals using a flapping motion for their thrust/lift generation and propulsion, which is made possible by the wings' inherent flexibility with this simplified model. We understand the existence of some discrepancies between the present study and live flying animals in the parametric map as one of our aims is to investigate this system dynamic response to the symmetry breakdown (see introduction for details). It is believed that the results obtained are still vital to elucidate the flexible wing propulsion mechanism.

The simulations show that the development history of lateral and rotational motion is similar to the studies of Spagnolie *et al* (2010) and Zhang *et al* (2010) for a two-dimensional foil and flat plate. In particular, the evolution follows left/right symmetry, an asymmetry, and eventually a stable forward or backward movement combined with a rotational pitching. However, our simulations of a low AR wing show that a 3D wing takes a longer developing history for breaking the symmetric flow structure around the wing, and reaching its final stable state than a 2D wing. Such a three-dimensional effect that is likely responsible for stabilizing force generation can also be observed in flying insects and maneuvering fish that fly or swim at low Reynolds numbers by flapping their wings or pectoral fins with low ARs as compared to those of bats and birds.

Analysis of the data within the fully developed flow regimes shows that the wing always pitches at the same frequency as forced flapping frequency, irrelevant to the wing's torsional stiffness and this is consistent with the study of Zhang *et al* (2010), which indicates that the low AR wing edge does not affect the dynamics of passive pitching in this aspect. On the other hand, for the lateral motion, both results show that the induced lateral velocity (Re_u) oscillating frequency is profoundly dependent on the wing torsional stiffness, varying from multiple frequencies to one dominant frequency with an increase in the wing's stiffness (figure 7 in the paper of Zhang *et al* (2010)). In addition, apart from mode B-2 where the Re_u frequency is double the flapping frequency found by

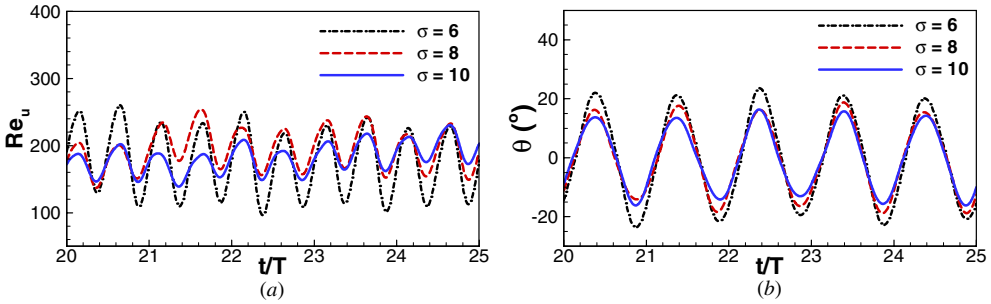

Figure 14. Density ratio effect on the evolution of $Re_{\rm u}$ and θ ($Re_{\rm fr} = 80$, AR = 2.0 and $F = 2.0$). (*a*) Induced non-dimensional lateral velocity $Re_{u.}$ (*b*) Induced pitching angle θ.

Zhang *et al* (2010) for their flat plate, we observed a mode B-1 state for our 2D wing, in which Re_u oscillating frequency appears to be the same as the flapping frequency. Considering the different parameters and geometry examined in the two studies, we can conclude that the dynamic response of such a flapping wing system is complicated, and very much dependent on the various system kinematic and structural parameters.

Further studies on the hydrodynamic performance of these wings in the fully developed state show that the wing AR, frequency ratio, density ratio and even the pitching axis have remarkable effects on their propulsion performance. The wings with large ARs always show large thrust force and thus a large Re_u than those of short spans. The vortex structure around the wing body shows that this is the result of a stronger reverse von Kármán vortex street generated in the wake of large ARs wing. In addition, we found that the stiffness influence on the wing propulsion is strongly linked to the pitching axis. Introduction of the pivot point away from chord-center to the leading edge leads to an improvement of propulsion performance. Further studies on this aspect would be our near future direction. In addition, the analysis of thrust force and efficiency relation with wing torsional stiffness shows that maximum thrust is generated when the wing flaps at its natural frequency, while the optimal efficiency is instead obtained if the wing flaps at half of its natural frequency. This conclusion remarkably resembles the observations from biological fliers, even though some parameters in the present study are beyond the range of that of real animals. Our results also show the predominant range for torsional stiffness impact on the propulsion of wing is between frequency ratios of $F = 1.0$ to 4.0.

References

Alben S and Shelley M J 2005 Coherent locomotion as an attracting state for a free flapping body *Proc. Natl Acad. Sci. USA* **102** 11163–6

ANSYS Inc. 2010 FLUENT 13 Documentation

Blondeaux P, Fornarelli F, Guglielmini L and Triantafyliou M 2005a Vortex structures generated by a finite-span oscillating foil *43rd AIAA Aerospace Sciences Meeting (Reno, Nevada, 10–13 Jan.)* pp 2005–84

Blondeaux P, Fornarelli F, Guglielmini L, Triantafyliou M and Verzicco R 2005b Numerical experiments on flapping foils mimicking fish-like locomotion *Phys. Fluids* **17** 113601

Borazjani I and Sotiropoulos F 2009 Numerical investigation of the hydrodynamics of anguilliform swimming in the transitional and inertial flow regimes *J. Exp. Biol.* **212** 576–92

Buchwarld R and Dudley R 2010 Limits to vertical force and power production in bumblebees (Hymenoptera: Bombus impatiens) *J. Exp. Biol.* **213** 426–32

Combes S A and Daniel T L 2003a Flexural stiffness in insect wings: I. Scaling and the influence of wing venation *J. Exp. Biol.* **206** 2979–87

Combes S A and Daniel T L 2003b Flexural stiffness in insect wings: II. Spatial distribution and dynamic wing bending *J. Exp. Biol.* **206** 2989–97

Dong H, Mittal R and Najjar F M 2006 Wake topology and hydrodynamic performance of low-aspect-ratio flapping foils *J. Fluid Mech.* **566** 309–43

Gazzola M, Van Rees W M and Koumoutsakos P 2012 C-start: optimal start of larval fish *J. Fluid Mech.* **698** 5–18

Hu J X and Xiao Q 2013 Three dimensional effects on the translational locomotion of a passive heaving wing *J. Fluids Struct.* (Minor revision)

Hu J X, Xiao Q and Incecik A 2011 Dynamic response of a flapping foil with a non-sinusoidal kinematic motion *Proc. 21st Int. Offshore and Polar Engineering Conf. (Maui, 19–24 June)* ed J S Chung, I Langen, S Y Hong and S J Prinsenberg (Maui: ISOPE) vol 2 p 239

Hunt J C R, Wray A A and Moin P 1988 Eddies, stream, and convergence zones in turbulent flows *Proc. 1988 Summer Program* (Stanford, CA: Center for Turbulence Research) pp 193–208

Ishihara D, Horie T and Denda M 2009 A two-dimensional computational study on the fluid–structure interaction cause of wing pitch changes in dipteran flapping flight *J. Exp. Biol.* **212** 1–10

Kang C K, Aono H, Cesnik C E S and Shyy W 2011 Effects of flexibility on the aerodynamic performance of flapping wings *J. Fluid Mech.* **689** 32–74

Kang C K and Shyy W 2013 Scaling law and enhancement of lift generation of an insect-size hovering flexible wing *J. R. Soc. Interface* **10** 85

Liu H 2005 Simulation-based biological fluid dynamics in animal locomotion *App. Mech. Rev.* **58** 269–81

Liu H, Nakata T, Gao N, Maeda M, Aono H and Shyy W 2010 Micro air vehicle-motivated computational biomechanics in bio-flights: aerodynamics, flight dynamics and maneuvering stability *Acta Mech. Sin.* **26** 863–79

Lu X Y and Liao Q 2006 Dynamic responses of a two-dimensional flapping foil motion *Phys. Fluids* **18** 098104

Montcastle A M and Combes S A 2013 Wing flexibility enhances load-lifting capacity in bumblebees *Proc. R. Soc.* B **280** 1759

Nakata T and Liu H 2012 Aerodynamic performance of a hovering hawkmoth with flexible wings: a computational approach *Proc. R. Soc.* **279** 722–31

Ramananarivo S, Godoy-Diana R and Thiria B 2011 Rather than resonance, flapping wing flyers may play on aerodynamics to improve performance *Proc. Natl Acad. Sci. USA* **108** 5964–9

Sane S P and Dickinson M H 2002 The aerodynamic effects of wing rotation and a revised quasi-steady model of flapping flight *J. Exp. Biol.* **205** 1087–96

Shyy W, Lian Y, Tang J, Viieru D and Liu H 2007 *Aerodynamics of Low Reynolds Number Flyers* (New York: Cambridge University Press)

Spagnolie S, Moret L, Shelley M J and Zhang J 2010 Surprising behaviors in flapping locomotion with passive pitching *Phys. Fluids* **22** 041903

Triantafyllou M S, Triantafyllou G S and Yue D K P 2000 Hydrodynamics of fishlike swimming *Annu. Rev. Fluid. Mech.* **32** 33–53

Vandenberghe N, Childress S and Zhang J 2006 On unidirectional flight of a free flapping wing *Phys. Fluids* **18** 014102

Vandenberghe N, Zhang J and Childess S 2004 Symmetry breaking leads to forward flapping flight *J. Fluid Mech.* **506** 147–55

Vanella M, Fitzgerald T, Preidikman S, Balaras E and Balachandran B 2009 Influence of flexibility on the aerodynamic performance of a hovering wing *J. Exp. Biol.* **212** 95–105

Willmott A P and Ellington C P 1997a The mechanics of flight in the hawkmoth Manduca sexta: I. Kinematics of hovering and forward flight *J. Exp. Biol.* **200** 2705–22

Willmott A P and Ellington C P 1997b The mechanics of flight in the hawkmoth Manduca sexta: II. Aerodynamic consequences of kinematic and morphological variation *J. Exp. Biol.* **200** 2723–45

Xiao Q, Sun K, Liu H and Hu J X 2011 Computational study on near wake interaction between undulation body and a D-section cylinder *Ocean Eng.* **38** 673–83

Zhang J, Liu N S and Lu X Y 2010 Locomotion of a passively flapping flat plate *J. Fluid Mech.* **659** 43–68

Zhang X, Ni S, Wang S and He G 2009 Effects of geometric shape on the hydrodynamics of a self-propelled flapping foil *Phys. Fluids* **21** 103302